ISET Journal of Earthquake Technology, Paper No. 598, Vol. 62, No. 2, June 2025, pp. 129-139

PHYSICAL MODELLING, SHAKING TABLE EXPERIMENTS, AND NUMERICAL SIMULATIONS OF SEISMIC ACTIONS ON RETAINING WALLS WITH DIFFERENT SUPPORT CONDITIONS

Rohit Tiwari*
Technical Design and Engineering, Transport for New South Wales, NSW 2152, Australia
& formerly at The University of New South Wales, Sydney, NSW 2052, Australia
Email id: rohit19862009@gmail.com

ABSTRACT

Earthquake response of base restrained and rotational base retaining wall is presented. Details of the scaled down modelling and the construction of the scaled down retaining wall models are also shown. Seismic performance of the scaled down models of base restrained and rotational base retaining wall is examined by conducting several shaking table experiments on them. Different high velocity pulse (HVPs) and string of pulses (multiple pulses) were applied at the base of both the retaining wall models to investigate their performance during the shaking table experiment. The results of shaking table experiments were than used to study the forced and free vibration response of the base restrained and rotational base retaining wall models. Finite element (FE) investigations were also carried out to understand the capability of the FE models to replicate the shaking table experiment results. Details to develop a robust FE model of the base restrained and rotational base retaining wall are also presented. During the shaking table experiments active and passive state movements were observed for both the retaining wall models. In the case of rotational base retaining wall, the dissipation of seismic forces resulted in its limited seismic movements, though the magnitudes of these movements are not insignificant.

KEYWORDS: Earthquake, Retaining Wall, Boundary Conditions, Shaking Table Experiment, Finite Element Model

INTRODUCTION

Earthquake induced damage and deformation of earth retaining structures is well known and studied by different researchers in the past (Shakal, 1994; Koseki et al., 1995). Seismic loading not only generates inertial forces in the retaining wall but also in the backfill supported by it. The amplified inertial forces in the backfill exerts significant seismic pressure on the retaining wall, triggering displacement and rotation of the retaining wall (Siddharthan et al., 1994). Due to their high stiffness, retaining walls and other earth retaining structures typically fail through excessive sliding and/or rotation (Crosariol, 2010; Callisto and Rampello, 2013). Pile foundations are profoundly used to support the retaining walls as they can transfer the retaining wall loads to the base soils or bed rock. The modern capacity design allows the formation of plastic hinges near the pile top. However, the plastic high formation in the piles can cause significant displacement and rotation of the retaining walls supported by them (Callisto and Rampello, 2013).

Earthquake response of prototype retaining walls can be investigated by conducting centrifuge or 1g shaking table experiments on their scaled down models. For replicating the realistic seismic performance of prototype retaining walls, their scaled down models need to satisfy different similitude criteria (Moncarz and Krawinkler, 1981). True scaled behaviour of the scaled down models can be achieved when excited using a centrifuge, however, the seismic centrifuge involves a complicated design with lesser possibility of repetitive testing. Moreover, the development and maintenance of the seismic centrifuge facility is expensive. On the other hand, use of 1g shaking tables to excite the scaled down models is popular amongst researchers due to the ease in 1g model construction, choice of different model sizes, and possibilities of repetitive testings. Although the 1g shaking table experiments on scaled down models are popular to study their seismic response, however, the 1g scaled down models are often subjected to the scaling issues which could affect their capability of replicating the realistic seismic performance of prototype geotechnical models (Moncarz and Krawinkler, 1981). Moreover, achieving the true model behaviour with 1g scale

https://doi.org/10.63898/FHJJ3590
*Corresponding Author

down models is not possible. However, reasonable response of the 1g scaled down models can be attained with the careful and robust scaled down modelling which involves the realistic considerations of (i) prototype material behaviour, (ii) applied loading, and (iii) boundary conditions (Moncarz and Krawinkler, 1981; Wood et al., 2012). The results of 1g shaking table experiments are not only useful for evaluating the earthquake response behaviour of prototype models but they can also be used to calibrate the complicated numerical models for ensuring the accuracy of numerical models.

In the present work, physical modelling of two scaled down retaining walls is presented. Among them one scaled down retaining wall is restrained at its base and the another can rotate about its base. Different shaking table experiments were performed on both the retaining wall models by exciting their base using different high velocity pulses (HVP) and multiple pulses. Earthquake response of both models was captured using several laser transducers and accelerometers. The role of backfill inertial forces on the maximum and residual seismic displacement of both the retaining wall models is investigated. Additionally, the effects of boundary conditions on the seismic displacements of retaining walls is explored. Details are shown to develop the robust and accurate finite element (FE) models of both the retaining walls considered for the shaking table experiment. The capability of the FE models is also verified for the replication of the shaking table experiment results.

SCALE DOWN MODELLING AND CONSTRUCTION OF SCALED DOWN RETAINING WALL MODELS

In the present study, two different scaled down retaining wall models are considered, one with a restrained base and the other with a rotational base. A dimensionless scaling factor (λ) of 10 is used for the similitude analyses on the prototype concrete retaining walls. Table 1 shows different scaling laws which were used for the scaling of geometry, material properties, and loading conditions of the prototype retaining wall models (Tiwari, 2020). As noted above, despite their high stiffness, the retaining walls and other earth retaining structures typically fail due to earthquake induced sliding and rotation, which happens much before the initiation of structural failure. Therefore, the requirement of same material in the scaled down retaining wall model is relaxed, this condition not only allows the use of appropriate material stiffness for the construction of the scaled down retaining wall model but also rule out the requirement of additional structural mass to satisfy the dynamic similitude conditions (Moncarz and Krawinkler, 1981). Based on a rigorous search the polycarbonate sheets were selected for the construction of the rotational base scaled down retaining wall model, as the young's modulus of polycarbonate ranges from 2-4 GPa. The rotation of the scaled down retaining wall about its base is achieved with the help of several rotational springs which were placed below the polycarbonate retaining wall base. The cumulative rotational stiffness of these springs represents a scaled down rotational stiffness of the prototype rock socketed pile foundations (Tiwari, 2020).

Due to the high flexibility and ability to deform during the shaking table experiment, a 4 mm thick Aluminium sheet was used for the construction of the base restrained retaining wall. Therefore, the scaled down model of the base restrained retaining wall should be considered as a distorted model, however, it can be used to study the (i) seismic displacement caused by the backfill inertial forces, (ii) model frequencies, and (iii) seismic behaviour of the backfill. Additionally, the shaking table experiment results of the base restrained retaining wall model were used to validate the seismic response of the FE models. Figure 1 shows the geometrical details of both the scaled down retaining wall models with restrained (Figure 1a) and rotational (Figure 1b) base, respectively. The detailed design of the scaled down model, along with the effects of reflecting and non-reflecting boundaries, has been previously presented by the author (Tiwari, 2020; Tiwari and Lam, 2021; Tiwari et al., 2026).

Crushed rock was used for the construction of backfill behind the retaining wall models. A detailed geotechnical testing was also carried out to characterize the backfill material. Different geotechnical properties of the crushed rock are given in table 2. The backfill was constructed in different layers, each layer was dynamically compacted using the shaking table vibrations. During the backfill compaction, the wall movements were restrained with the help of external clamps. Figure 2 shows the constructed scaled down retaining wall models with restrained (Figure 2a) and rotational (Figure 2b) base.

Table 1: Similitude laws considered for the scale down modelling

	Prototype model	1g Scaled down model
Length or Depth	L or D	L/λ or D/λ
Acceleration	A	A
Stress	σ'	σ'/λ
Stiffness	G or E	G/λ^{α} or E/λ^{α}
Strength	s_u	s_u/λ
Velocity	V	$V/\lambda^{1-\alpha/2}$
Time	t	$t/\lambda^{1-\alpha/2}$
Frequency	f	$f\lambda^{1-\alpha/2}$
Displacement	U	$U/\lambda^{2-\alpha}$

Table 2: Geotechnical properties of the backfill (crushed rock)

Sr. No.	Crushed rock property	Value (Unit)
1.	Maximum dry density	1790 kg/m^3
2.	D_{60} size	6 mm
3.	D_{30} size	4.2 mm
4.	Constrained modulus	2.5 MPa (for $\sigma_v = 7$ kPa)
5	Young's modulus	2.9 MPa (for $\sigma_c = 7$ kPa)
6.	The angle of internal friction	44°
7.	Poisson's ratio	0.45
8.	Dilation angle	19°.

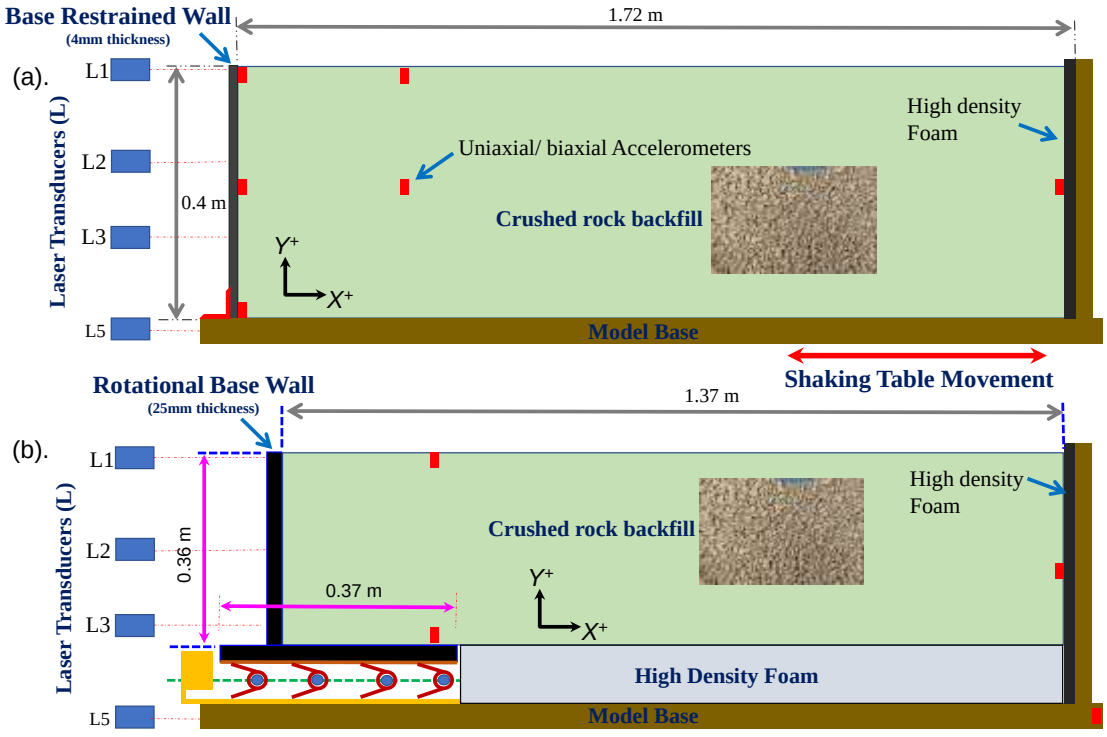

Fig. 1 Base restrained (top) and rotational base (bottom) models of the scaled down retaining walls

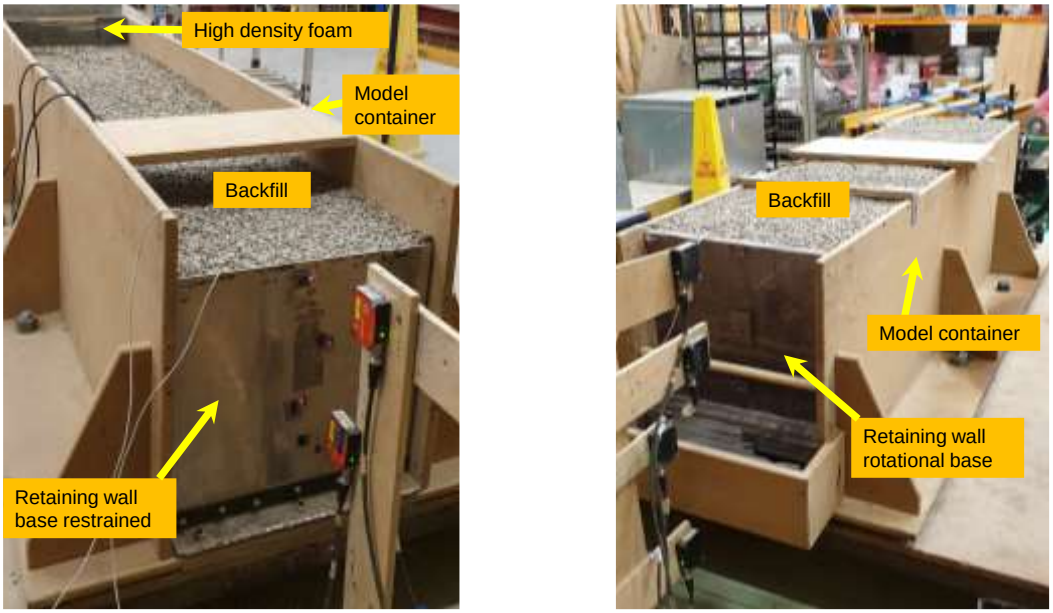

(a) Base restrained retaining wall model (b) Rotational base retaining wall model

Fig. 2 Constructed scaled down retaining wall models

INSTRUMENTATION SETUP AND SELECTION OF INPUT EXCITATIONS

To capture the seismic response of both the scale down retaining wall models a robust instrumentation setup was planned and implemented. Several high precision laser transducers were used to capture the displacement of retaining wall models and shaking table base. Additionally, several uniaxial and biaxial accelerometers were also inserted inside the backfill to capture its seismic response. Output frequency of the instruments was kept sufficiently low to capture the important earthquake responses of the scaled down retaining wall models.

The earthquake response of both the retaining wall models was analysed using several HVP and two multiple pulses. Figure 3 shows a typical input HVP used for the shaking table experiments on the scaled down retaining wall models. Figure 4 shows different multiple pulses used for the shaking table experiment on the scaled down retaining wall models. Due to the higher flexibility of the base retained retaining wall, it was excited using the multiple pules with maximum applied displacement ($MP_{\text{A-Max}}$) of 20 and 25 mm, and applied frequency (f_{Applied}) of 3 Hz (Figure 4 top). Two multiple pulses with $MP_{\text{A-Max}}$ of 11 and 13 mm and f_{Applied} of 4 Hz were used to excite the rotational base retaining wall (Figure 4 bottom).

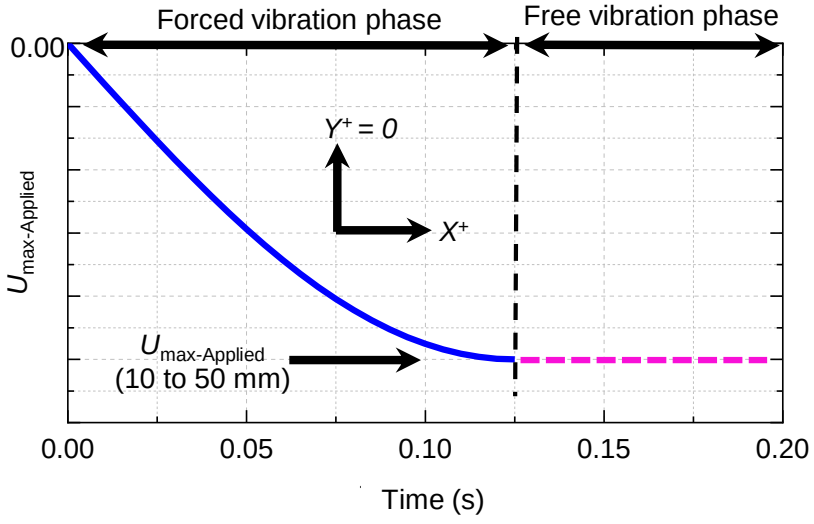

Fig. 3 Typical input HVP used for the shaking table experiment

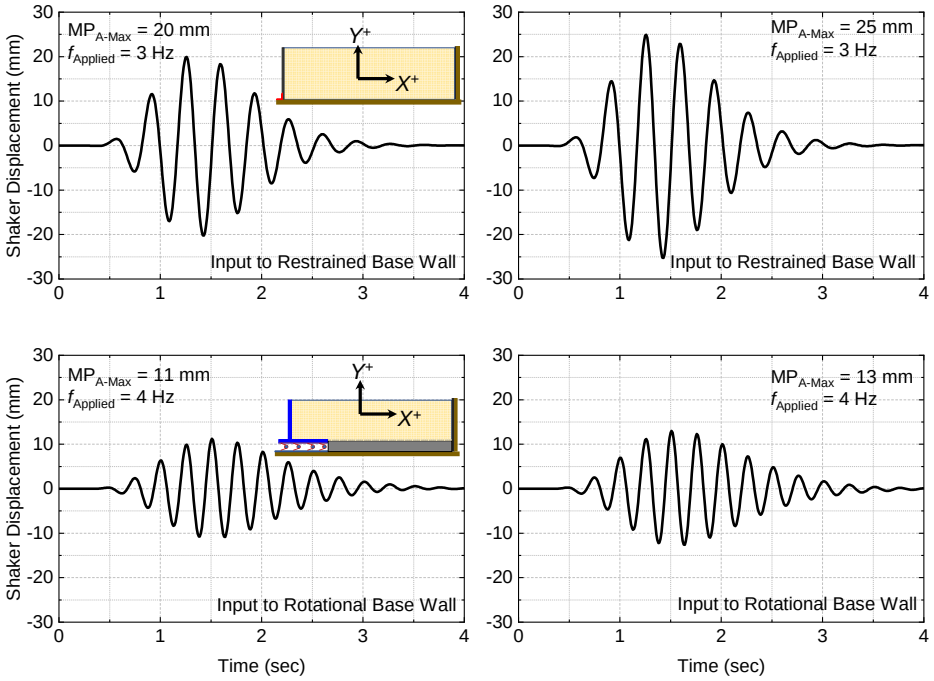

Fig. 4 Input multiple pulses for the shaking table experiments

DISCUSSION ON THE SHAKING TABLE EXPERIMENT RESULTS

1. Displacement Response of the Scaled Down Retaining Wall Models

Displacement response of both the scaled down retaining wall models is analysed when their base was excited with different HVPs. Figure 5a and 5b shows the maximum relative displacements (Δ_{Rel})

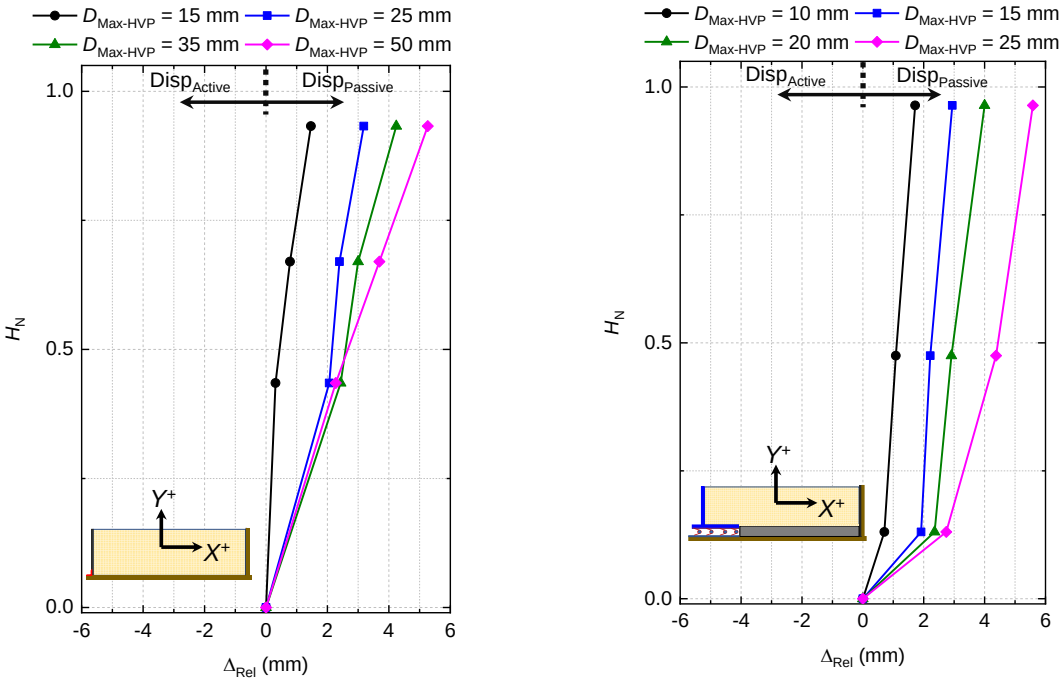

(a) Maximum Δ_{Rel} along the base restrained retaining wall height

(b) Maximum Δ_{Rel} along the rotational base retaining wall height

Fig. 5 Maximum Δ_{Rel} of the retaining walls during the forced vibration phase

captured during the forced vibration phase for the base restrained and rotational base retaining wall respectively. The Δ_{Rel} is shown at different normalized heights (H_N), when the H_N equals to 1, it represents the retaining wall top, and when the H_N equals to 0, it represents the retaining wall base. Effect of backfill inertial forces on the seismic displacement of the base restrained retaining wall can be observed from Figure 5a. A nonlinear passive state seismic displacement of the base restrained retaining wall is observed above the mid retaining wall height which is also the point of seismic backfill force. The scaled down retaining wall with rotational base shown linear passive state movement for all input HVPs, with magnitudes nearly 100% higher than the passive movements observed in the base restrained retaining wall. The higher passive displacements of the rotational base retaining wall highlights the importance of considering the role of foundation ductility into the seismic retaining wall design.

Figure 6a and 6b shows the residual Δ_{Rel} at different H_N for the base restrained and rotational base retaining wall respectively. The base restrained retaining wall shown significant nonlinear residual Δ_{Rel} in the active direction. Soon after the commencement of the HVP, both the retaining walls and their backfill shown inertial effects by moving opposite (passive direction) to the direction of the base movement (active direction). However, before the completion of the forced vibration phase the retaining walls and the backfill started moving in the direction of the base movement (active direction) which resulted in a gap formulation between the retaining wall stem and the backfill.

The high flexibility of the base restrained retaining wall resulted in a larger gap formulation. Soon after the gap formation the backfill fell on the base restrained retaining wall, resulting in a higher active residual Δ_{Rel} which increases with the increasing magnitude of the HVP. In the case of rotational base retaining wall, soon after the commencement of HVP, the compressed rotational springs beneath the retaining wall undergo decompression due to the passive movement of the retaining wall stem (Figure 5b) which resulted in the limited gap formation between the retaining wall stem and backfill. This action also dissipated the seismic force in the retaining wall and backfill due to the mobilization of backfill's passive resistance, resulted in lesser residual Δ_{Rel} of the rotational base retaining wall.

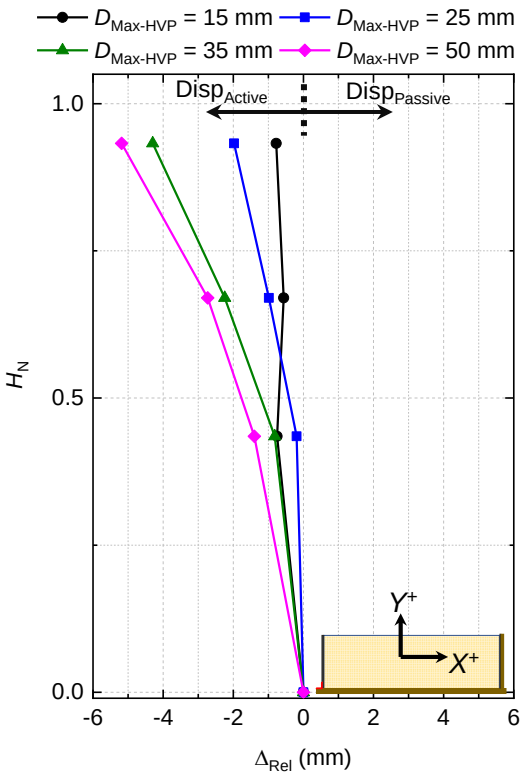

(c) Residual Δ_{Rel} along the base restrained retaining wall height

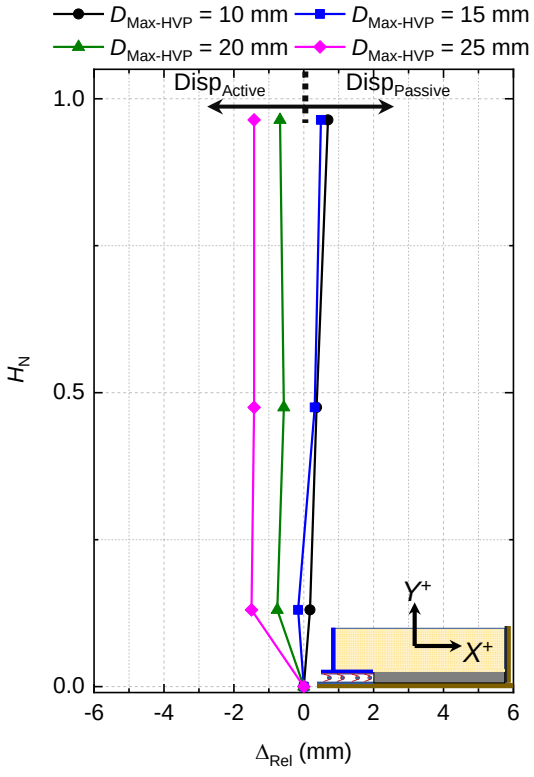

(d) Residual Δ_{Rel} along the rotational base retaining wall height

Fig. 6 Residual Δ_{Rel} of the retaining walls after the completion of HVPs

Figure 7 shows the Δ_{Rel} time history of the base restrained retaining wall for different H_N (Tiwari and Lam, 2021). Active movement of the base restrained retaining wall can be observed for both the input

multiple pulses, moreover, significant residual Δ_{Rel} at different H_N. can be observed. This highlights the role of backfill inertial forces on the active movement of retaining walls.

Figure 8 shows the Δ_{Rel} time history for the rotational base retaining wall for different H_N. Unlike the base restrained retaining wall, passive movements of the rotational base retaining wall can be observed during 1 to 2 seconds of the ground excitation. On completion of input excitation, the rotational base retaining wall also demonstrated active residual Δ_{Rel}. Although the rotational base retaining wall was excite using higher input pulse frequency, its residual Δ_{Rel} are closer to the residual Δ_{Rel} of the base restrained retaining wall. Therefore, It can be concluded that the passive rotation of the rotational base retaining wall can dissipate the seismic forces by mobilizing the passive resistance of the backfill.

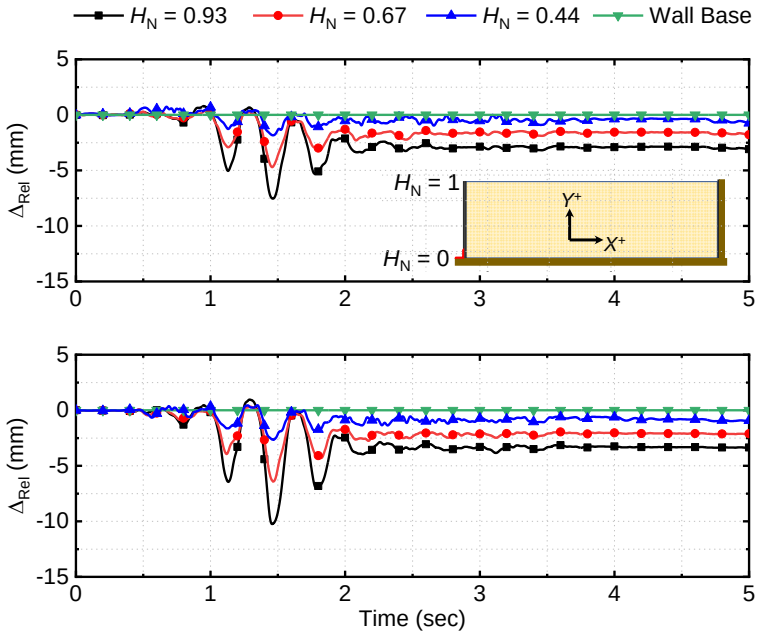

Fig. 7 Δ_{Rel} time history at different H_N of the base restrained retaining wall

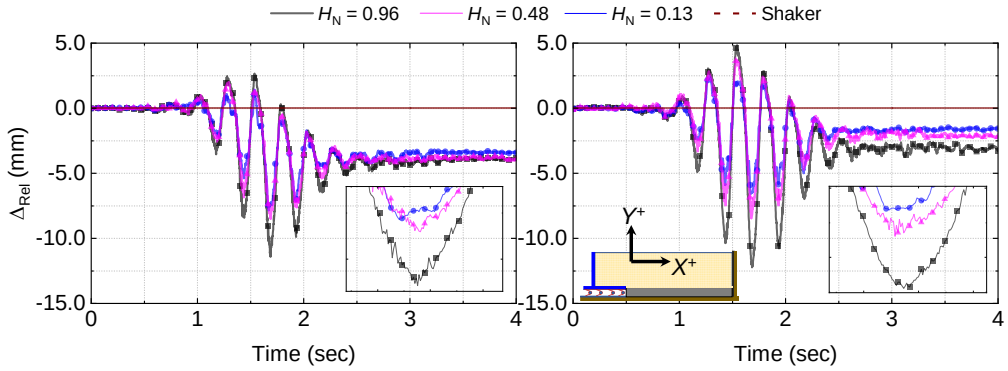

Fig. 8 Δ_{Rel} time histories at different H_N of the rotational base retaining wall

2. Estimation of the Model Frequencies and Shear Wave Velocity in the Backfill

The free vibration response of both the retaining wall models was analysed using the captured backfill top accelerations, when the shaking table base was excited using different HVPs. Frequency domain analyses were performed on the captured backfill accelerations based on which the 1st natural frequencies (f_n) of the base restrained and rotational base retaining wall was estimated as 20 Hz and 27 Hz, respectively. Higher flexibility of the base restrained retaining wall resulted in its lower natural frequency. The shear wave velocity (V_S) in the backfill was also estimated using the lateral backfill accelerations (A_x), which were captured at different backfill heights when the model base was excited using the multiple pulses. The time lag between the backfill accelerations at modal base and backfill top was estimated during the initial

loading cycles, based on which the shear wave velocity in the base restrained retaining wall backfill was estimated as 31 m/sec. Due to the high noises captured in the acceleration data the shear wave velocity (for the first modal period) for the rotational base retaining wall is determined using the analytical expression ($V_S = 4Hf_n$) and estimated as 39 m/sec.

DEVELOPMENT OF THE FE MODELS OF THE SCALED DOWN RETAINING WALLS

1. Geometrical Modelling

Two dimensional (2D) plane strain (PS) FE models of the scaled down retaining walls are developed in the FE software Abaqus. Figure 1 shows the dimensional details of both the scaled down retaining walls. Different model parts were developed and meshed separately and later assembled according to the geometrical requirements. The FE mesh was generated using the 2D, PS, element CPE4R available in the Abaqus explicit. The reduced integration scheme with hourglass control and second order accuracy was also adopted in the selected FE element to ensure the effectiveness and accuracy of the FE analyses.

2. Material Modelling

Accurate modelling of the backfill's constitutive behaviour was achieved with the help of different geotechnical testings, which were carried out on the crushed rock. The backfill is modelled using the extended Mohr-Coulomb material model available in the FE software Abaqus. To simulate the post yield behaviour of the backfill, a separate calibration was conducted using the consolidated drained (CD) triaxial test results. Damping in the backfill was also modelled using the Rayleigh damping model inbuilt in the FE software Abaqus. The mass and stiffness dependent coefficients of the Rayleigh damping model were determined using the estimated shear wave velocity in the backfill. Details of different geotechnical testings, calibration of the extended Mohr-Coulomb material model, and Rayleigh damping model is previously presented by the Author (Tiwari and Lam, 2021; 2022). Except for the backfill soil, all other parts of both the retaining walls were modelling using the elastic material properties as given in table 3. The properties of the backfill are given in table 2 and 3.

Table 3: Material properties for the FE model

Sr. No.	Material	Density (Kg/m^3)	Elastic Modulus (Gpa)	Poisson's Ratio
1.	Aluminium	2700	69	0.33
2.	Polycarbonate	2400	2.6	0.3
3.	Steel	7800	200	0.3
4.	Wood	1000	100	0.3
5.	Foam	2000	0.1	0.4

3. FE solution Scheme, Interaction Modelling, and Boundary Conditions

The nonlinear time history FE analyses were performed using the Abaqus explicit module which is capable in solving the boundary value problems which involves moderate to large mesh deformations. Abaqus explicit uses a central difference method to solve the equation of motion through a stable time increment. The minimum time required for any stable time increment can be estimated by diving the smallest element length with the dilatational wave velocity. To avoid the aliasing in the FE results, the output frequency of the requested output quantities was selected as 1/10th of the time step of the input ground excitation. The interaction between backfill - retaining wall and backfill - model side/base was simulated by assigning frictional contact in the tangential direction and hard contact in the normal direction. Coefficient of friction of 0.64 and 0.45 was used for the base restrained and rotational base retaining wall, respectively. For the base restrained retaining wall, the wall base is restrained with the model container using the steel angle sections. For rotational base retaining wall, the rotational springs are modelled using the equivalent nonlinear vertical springs. The stiffness and damping of the nonlinear springs were calibrated with different FE iterations. The base of the FE models was assigned roller boundary conditions by restricting its vertical (y) movement and allowing the translation in the lateral directions (x). The multiple pulses as shown in figure 4 were applied to excite the FE model base. The effects of mesh convergence and different boundary conditions are previously addressed by the author (Tiwari and Lam, 2021). Figure 9 shows the developed FE model of the base restrained (Figure 9a) and rotational base (Figure 9b) retaining wall.

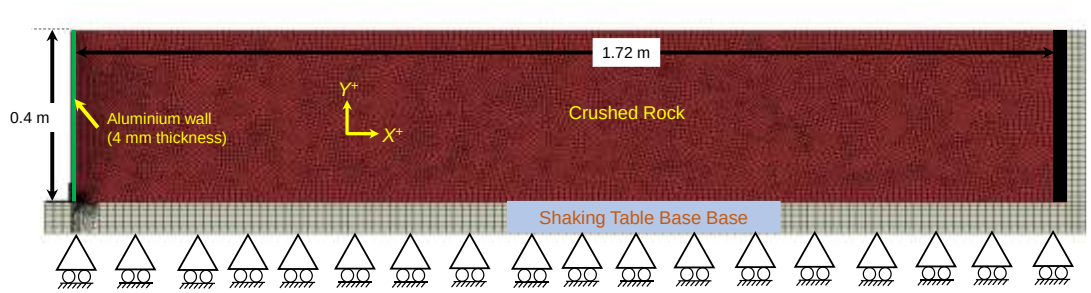

(a) FE model of the base restrained retaining wall.

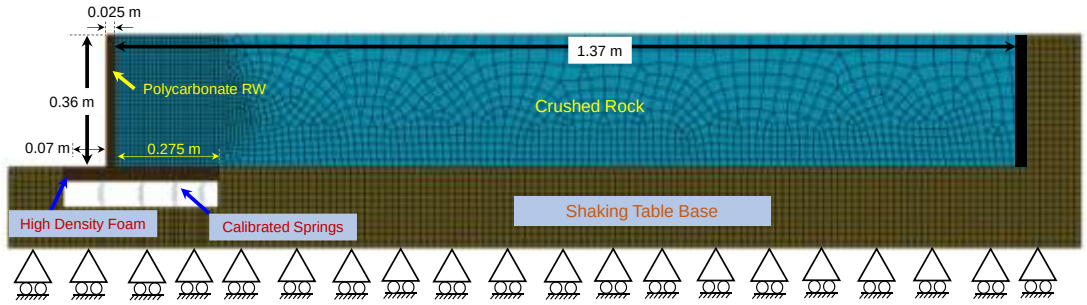

(b) FE model of the rotational base retaining wall.

Fig. 9 Developed FE models of the base restrained and rotational base retaining walls

COMPARISONS BETWEEN THE FE MODEL AND SHAKING TABLE EXPERIMENT RESULTS

Figure 10 shows the comparison of Δ_{Rel} of base restrained retaining wall (at H_N = 0.93), as captured during the shaking table experiments and simulated using the FE analyses, when excited using $MP_{A\text{-}Max}$ = 20 and 25 mm and $f_{Applied}$ = 3 Hz, respectively. Figure 10a and 10b shows the comparison when damping was not considered in the FE analyses, Figure 10c and 10d shows the comparison when the Rayleigh damping was considered in the backfill. A good agreement between the shaking table experiment results and FE simulations was observed.

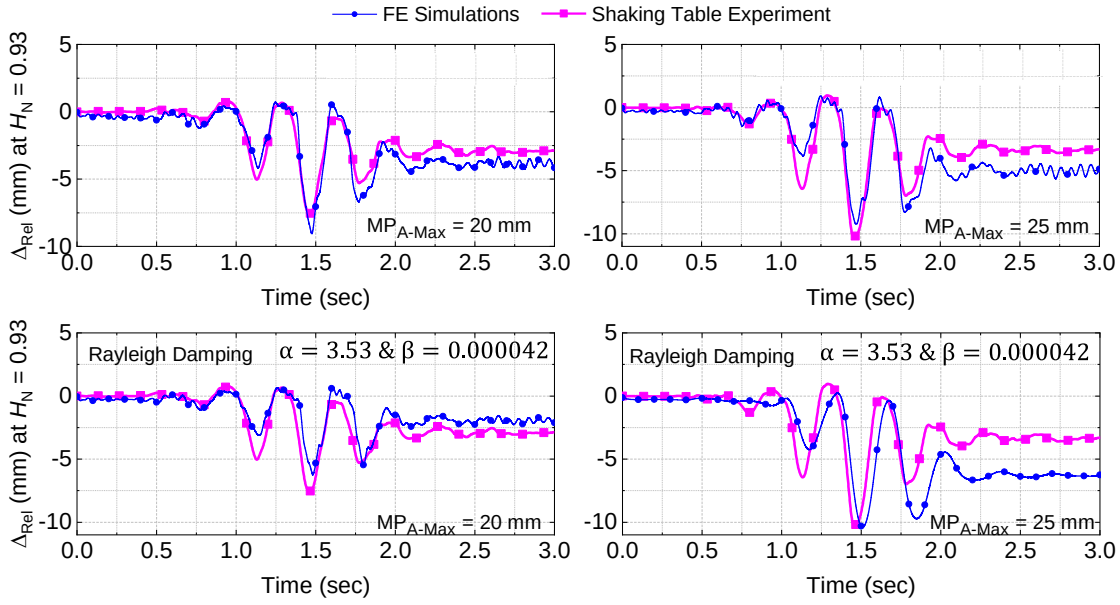

Fig. 10 Comparison of Δ_{Rel} of base restrained retaining wall as observed during the shaking table experiment and simulated using the FE analyses (Tiwari and Lam, 2021)

Figure 11 shows the comparison of the Δ_{Rel} of rotational base retaining wall (at H_N = 0.96), as captured during the shaking table experiment and simulated using the FE analyses when excited using $MP_{A\text{-}Max}$ = 11 and 13 mm and $f_{Applied}$ = 4 Hz, respectively. Despite of using severe ground shaking to excite the scaled down models, good agreement between the shaking table experiment results and FE simulations can be observed. Figure 12 shows the comparison of A_x (at backfill top) as captured during the shaking table experiment and simulated using the FE analyses, when excited using $MP_{A\text{-}Max}$ = 11 and 13 mm and $f_{Applied}$ = 4 Hz. Again, good agreement is demonstrated between the shaking table experiment results and FE simulations.

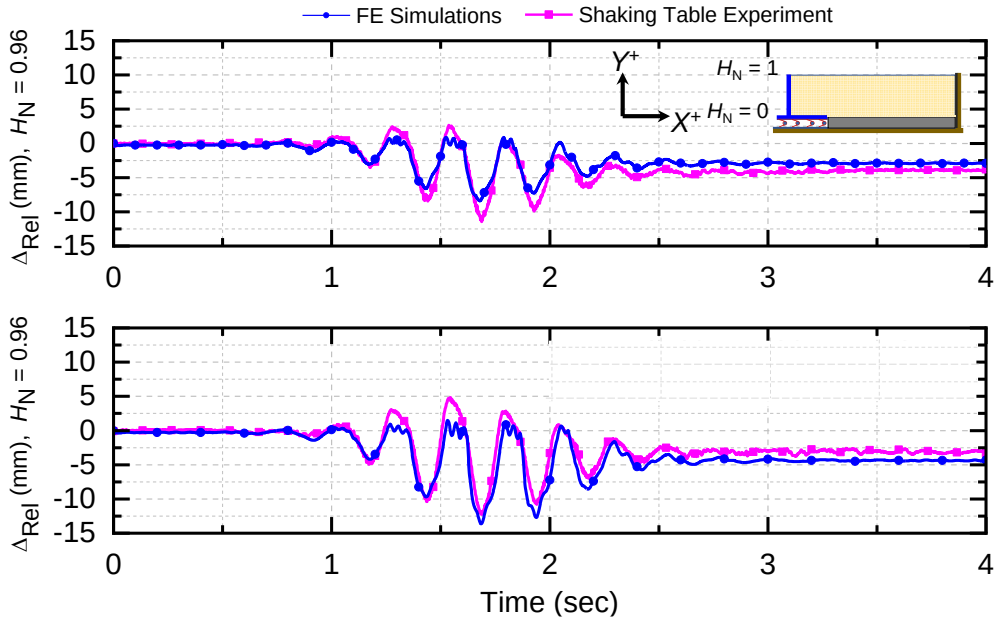

Fig. 11 Comparison of Δ_{Rel} of rotational base retaining wall as observed during the shaking table experiment and simulated using the FE analyses

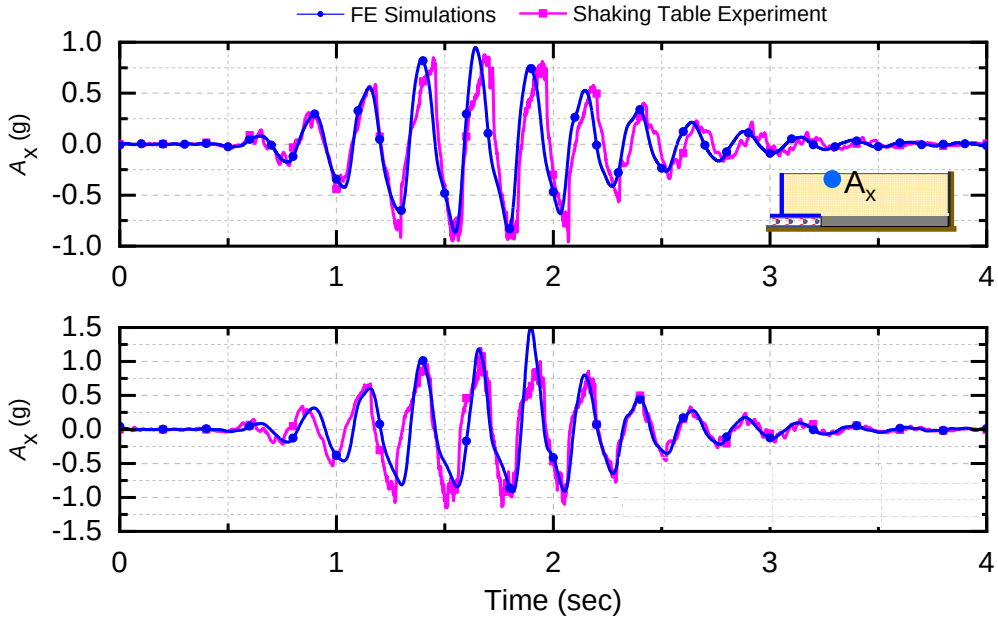

Fig. 12 Comparison of Ax at the top of the backfill of rotational base retaining wall, as observed during the shaking table experiment and simulated using the FE analyses

CONCLUSIONS

Seismic performance of the base restrained and rotational base retaining wall is studied. Details of the scaled down modelling and scaled down model construction are also shown. A detailed shaking table experiment was performed on both the retaining wall models by exciting their base with different HVPs and multiple pulses. The results of shaking table experiments were presented for the forced and free vibration responses of both the retaining wall models. Development of 2D FE models of the base restrained and rotational base retaining wall is also shown and their capability for replicating the shaking table experiment results was also verified. Following conclusions were made:

1. Backfill induced inertial forces can significantly influence the maximum and residual seismic displacement of the base restrained and rotational base retaining wall.
2. The movement of retaining walls during and after an earthquake is significantly influenced by their boundary conditions. When excited using the HVPs the base restrained retaining wall shown nonlinear Δ_{Rel} along its height, however, the rotational base retaining wall shown linear Δ_{Rel} along its height.
3. When excited using HVPs, the rotational base retaining wall shown lesser residual Δ_{Rel} along its height, which is due to the higher dissipation of earthquake forces during its passive movements.
4. Active residual Δ_{Rel} of both the retaining walls was observed when excited using the multiple pulses, however, due to the passive displacement capability, the rotational base retaining wall shown limited residual Δ_{Rel}, despite higher input excitation frequency.
5. The developed FE models of the base restrained and rotational base retaining walls can effectively replicate the seismic performance of their physical models.

REFERENCES

1. Callisto, L. and Rampello, S. (2013). "Capacity Design of Retaining Structures and Bridge Abutments with Deep Foundations", Journal of Geotechnical and Geoenvironmental Engineering, Vol. 139, No. 7, pp. 1086-1095.
2. Crosariol, V.A. (2010). "Scale Model Shake Table Testing of Underground Structures in Soft Clay", *Master of Science Thesis, California Polytechnic State University, USA*.
3. Koseki, J., Tateyama, M., Tatsuoka, F. and Horii, K. (1995). "Back Analyses of Soil Retaining Walls for Railway Embankments Damaged by the 1995 Hyogoken-Nanbu Earthquake", *Joint Report*, pp. 31-56.
4. Moncarz, P.D. and Krawinkler, H. (1981). "Theory and Application of Experimental Model Analysis in Earthquake Engineering", *the John A. Blume Earthquake Engineering Center, Stanford University, California, USA.*
5. Shakal, A.F. (1994). "CSMIP Strong-Motion Records from the Northridge", *California earthquake*.
6. Siddharthan, R., El-Gamal, M. and Maragakis, E.A. (1994). "Investigation of Performance of Bridge Abutments in Seismic Regions", *Journal of Structural Engineering, ASCE,* Vol. 120, No. 4, pp. 1327-1346.
7. Tiwari, R. (2020). "Displacement Based Seismic Assessment of Earth Retaining Structures", *Doctoral Thesis, the University of Melbourne, Australia*.
8. Tiwari, R. and Lam, N. (2021). "Modelling of Seismic Actions in Earth Retaining Walls and Comparison with Shaker Table Experiment", *Soil Dynamics and Earthquake Engineering,* Vol. 150, pp. 106939.
9. Tiwari, R. and Lam, N. (2022). "Displacement Based Seismic Assessment of Base Restrained Retaining Walls", *Acta Geotechnica*, Vol. 17, No. 8, pp. 3675-3694.
10. Tiwari, R., Jimenez, A. and Russell, A.R. (2026). "Seismic Response of Sand Beds in A Laminated Shear Stack: Physical and Numerical Modelling", *Soil Dynamics and Earthquake Engineering, pp. 200(Part A).*
11. Wood, D.M., Crewe, A. and Taylor, C. (2002). "Shaking Table Testing of Geotechnical Models", *International Journal of Physical Modelling in Geotechnics Mar*, Vol. 2, No. 1, pp. 01-13.